ELSEVIER

Materials Science and Engineering A 435–436 (2006) 163–171

MATERIALS SCIENCE & ENGINEERING A

www.elsevier.com/locate/msea

An enhanced age hardening response in Mg–Sn based alloys containing Zn

C.L. Mendis [a], C.J. Bettles [a,b,*], M.A. Gibson [b], C.R. Hutchinson [a]

[a] *ARC Centre of Excellence for Design in Light Metals, Department of Materials Engineering, Monash University, Clayton 3800, Victoria, Australia*

[b] *CAST CRC-CSIRO Manufacturing and Infrastructure Technology, Private Bag 33, Clayton South MDC, Clayton 3169, Victoria, Australia*

Received 31 May 2006; accepted 21 July 2006

Abstract

Additions of Zn and Zn + Na to an age hardenable Mg–1.3 Sn (at.%) alloy have been examined using hardness measurements and transmission electron microscopy. Zn additions resulted in a substantial increase (300%) in the hardening increment after aging at 200 °C but the time to peak hardness was relatively unaffected. The additions were found to have little effect on the number density of precipitates formed and no effect on the identity of precipitates but significant changes to particle morphology were observed. Combined additions of Zn and Na (an element previously illustrated to be an effective microalloying element for the Mg–Sn system) showed features typical of separate additions of Na and Zn: a large increase in the observed hardening increment, an acceleration of the time to peak hardness and a change in particle morphology. Furthermore, the combined Zn + Na additions resulted in synergistic effects on precipitate stability during overaging and the time to peak hardness. The stability of Mg_2Sn precipitates formed in the Mg–Sn–Zn–Na alloy was much greater than those usually observed in the Mg–Sn–Na system and the time to peak hardness was much reduced from ∼58 h in the Mg–Sn–Na alloy to 7 h in the Mg–Sn–Zn–Na alloy.

Keywords: Precipitation; Magnesium alloys; Morphology; Transmission electron microscopy

1. Introduction

The worldwide emphasis on increased fuel efficiency in automobiles has thrust magnesium alloys into the fore as potentially lightweight materials for structural applications. It is expected that this trend in lightweighting automobiles will continue and if suitable magnesium alloys can be developed they will substitute for their heavier Al and steel based counterparts. In particular, there is currently much research into the development of magnesium based alloys for powertrain applications. Applications in transmission housings and crankcases require high performance at elevated temperatures (>150 °C) and under these conditions the stability of microstructure (and therefore properties) is of key importance. Those alloys that derive their strength from precipitation hardening are usually considered the most promising for such applications and the thermal stability of the precipitate distribution is an important component of the overall microstructural stability.

One alloy system that may show some promise in elevated temperature applications is the Mg–Sn system. This is an age hardenable system with the potential to form ∼10 vol.% of Mg_2Sn. The Mg_2Sn precipitate (FCC, $a = 0.676$ nm, point group $m\bar{3}m$) [1] has a high melting temperature (∼770 °C) and alloys based on this system are thought to show some promise for use in applications requiring elevated temperature creep resistance [2]. Van der Planken [3] considered the hardening response of an Mg–1.65 Sn (at.%) alloy at 200, 250 and 300 °C using microhardness tests and, despite the relatively large fraction of Mg_2Sn particles formed, the hardening response was very low. Derge et al. [4] examined the orientation relationship between the Mg matrix and the Mg_2Sn equilibrium phase using X-ray diffraction and optical microscopy techniques. They reported that the Mg_2Sn phase forms with a plate-like morphology and that a variety of orientation relationships exist depending on the formation temperature. Mendis et al. [5] have recently examined a similar alloy aged at 200 °C, which confirmed the poor age hardening response in the binary alloy and, using transmission electron microscopy observations, reported that the Mg_2Sn phase forms with a lath-shaped morphology on the $(0\,0\,0\,1)_{Mg}$ basal planes of the matrix with the following orientation relationship

* Corresponding author. Tel.: +61 3 9905 1966; fax: +61 3 9905 4940.
E-mail address: colleen.bettles@eng.monash.edu.au (C.J. Bettles).

0921-5093/$ – see front matter © 2006 Elsevier B.V. All rights reserved.
doi:10.1016/j.msea.2006.07.090

(OR):

$$\{1\,1\,1\}_{Mg_2Sn}//(0\,0\,0\,1)_{Mg} \text{ and } \langle 1\,1\,0\rangle_{Mg_2Sn}//\langle 1\,1\,\bar{2}\,0\rangle_{Mg} \quad (1)$$

In efforts to increase the strength of precipitation hardenable alloys there has been a general emphasis on the refinement of the scale of the particle distribution [6–8]. The strategies have mostly concentrated on increasing the precipitate nucleation rate so that the number density of particles is increased, leading to a smaller average interparticle spacing, λ, and a larger Orowan stress for particle by-passing, $\sigma_p \approx Gb/\lambda$ (G is the shear modulus of the matrix and b is the Burgers vector). The use of microalloying additions for this purpose has been particularly well studied in age hardenable Al alloys [9,10]. Examples include In, Cd or Sn additions to Al–Cu alloys [11–14], which give rise to a refined distribution of θ' precipitates, and Ag + Mg additions to Al–Cu alloys which both refine the particle distribution and alter the habit plane on which the precipitates form [15,16].

Mendis et al. [5] recently proposed a qualitative thermokinetic criteria for choosing microalloying additions for precipitation hardenable alloys. This framework was used to select Na and In + Li additions as potentially useful microalloying elements for the Mg–Sn based system and this usefulness was confirmed experimentally. Na additions to a Mg–1.3 Sn (at.%) alloy were found to increase the number density of Mg_2Sn precipitates formed at 200 °C by two orders of magnitude, resulting in a 270% increase in the hardening increment from precipitation. In the case of In + Li additions, the increase in number density was closer to one order of magnitude and the hardening increment was ~150%. For elevated temperature applications, where microstructural stability is an important consideration, this approach to increasing the strength of Mg based alloys may suffer from an important disadvantage. For a given volume fraction of precipitates, increases in the number density of precipitates necessarily corresponds to a decrease in the mean particle size. The driving force for coarsening processes is the excess energy stored in the particle/matrix interfaces and the coarsening rate, dR/dt, of a particle distribution scales as $1/R^2$ [17–19]. Thus, the increase in strength of precipitation-hardened alloys through refinements in scale may come at the cost of a decrease in the thermal stability of the precipitate distribution.

An alternative, albeit more ambitious, approach to increasing the strength of precipitation hardenable Mg based alloys takes advantage of the anisotropy of crystallographic slip in the HCP lattice and emphasises changes in particle shape and/or orientation rather than scale [20]. At temperatures below 200 °C, the primary mode of deformation in Mg is by slip on the basal planes [21]. The effectiveness of precipitates at inhibiting basal slip depends not only on the mean particle size and number density, but also on the particle shape with respect to the basal slip plane. The dependence of the precipitate strengthening contributions in Mg alloys on particle morphology has been discussed by Nie [22]. For a given particle size and number density, the most efficient particle morphology for inhibiting basal slip will be that which is elongated in directions perpendicular to the basal plane (such as plates formed on the prismatic planes of the matrix), thus maximizing the probability that a gliding dislocation will intersect the precipitate. The least efficient particle morphology will be that which leads to elongation in directions within the basal plane, thus minimizing the probability of a dislocation intersecting the precipitate. In the Mg–Sn system at temperatures around 200 °C, the Mg_2Sn precipitate forms as thin laths on the basal plane, i.e. in an unfavourable orientation for blocking basal slip. If the morphology, orientation relationship or aspect ratios of these precipitates could be altered, without a significant reduction in the mean particle size, then substantial increases in strength might be realized without sacrificing the potential thermal stability of the particle distribution.

Unfortunately, the factors controlling the development of particle morphology in the solid state are not quantitatively understood. One school of researchers (i.e. the crystallographers, e.g. [23–26]) has emphasized the role of variations on structural matching of the matrix and precipitate lattices across the interface in controlling the development of particle morphology. Although this purely geometric approach is likely to be only part of the story (it ignores the chemical contribution to the interface energy, the mass transfer that accompanies interface motion as well as considerations of the magnitude of the driving force causing the interface to move) it has had some success in rationalizing the orientation relationships and habit planes of some precipitates in selected systems [24,25]. One factor that has been shown to be of importance in determining precipitate morphology is the ratio of lattice parameters of the matrix and the precipitate. The effect of a selection of alloying additions on the lattice parameters of HCP Mg [27] are shown in Fig. 1.

Ag and Zn are the two elements shown to have the largest effect on the lattice parameter of Mg. Derge et al. [4] reported that in the binary Mg–Sn system a variety of orientation relationships could be observed depending on the transformation temperature, suggesting that the relationship usually observed at 200 °C (Eq. (1)) may not represent an extremely deep minimum in energy. Zn has been chosen as a potentially interesting alloy addition because reasonable solid solubility is expected, it is a relatively inexpensive element and it is not expected to cluster with Sn on the HCP lattice thereby substantially modifying the nucleation of Mg_2Sn. Additions of the order of 1 at.% are expected to result in variations in the lattice parameter of HCP Mg of an absolute magnitude comparable to the changes due to the thermal expansion of the HCP lattice over ~200 °C (approximate temperature range considered by Derge et al.). If the ratio of the lattice parameters of the matrix and precipitate phases is an important factor in controlling precipitate shape and/or orientation, then Zn additions of this magnitude, purely from a geometric point of view, may be expected to have some interesting effects.

Variations in the bulk chemistry of the Mg–Sn based alloy will have an effect on the thermodynamic driving force for Mg_2Sn precipitation (and other potentially competing phases) as well as the precipitate/matrix interfacial energy. Both factors are expected to affect the nucleation rate of Mg_2Sn precipitates. The hope is that this is a second order effect and the first order effect is a significant variation in either the shape or aspect ratios of Mg_2Sn precipitates or their orientation with respect to dislocation glide on the basal planes. The objective is to exploit effects

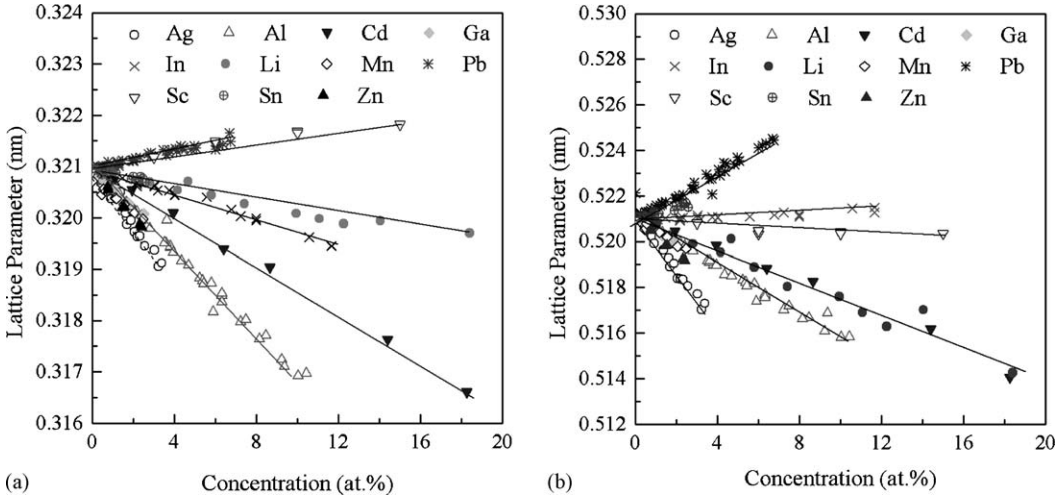

Fig. 1. The effect of alloying additions in solid solution on the (a) *a* and (b) *c* lattice parameters of magnesium.

of changes in particle shape (with respect to the gliding basal dislocations) rather than particle scale to increase the strength of these alloys.

In addition, the possible cumulative effects of Zn and Na additions are tested in this work. Na has previously been shown to be a potent microalloying addition in the Mg–Sn system resulting in a substantial refinement of the Mg_2Sn particle distribution [5]. The objective of using both Zn and Na additions is to test the possibility of simultaneously tailoring changes in particle shape (with respect to the basal plane) and scale.

2. Experimental procedure

A total of four alloys were prepared and the compositions are summarized in Table 1.

The compositions were each prepared from high purity Mg (99.9%), Sn (99.9%), Zn (99.9%) and a Sn–11.8 Na (at.%) master alloy in quantities of ~50 g. The alloys were induction melted in mild steel crucibles in an argon atmosphere and cast into a mild steel mould coated with a layer of carbon graphite held at approximately 300 °C. All alloys were encapsulated in Pyrex tubes, partially pressurised with high purity Ar, for homogenization treatments. They were heat treated at 345 °C for 2 h, to dissolve low temperature melting phases that may have formed, prior to heating to 500 °C at a heating rate of 1.3 °C/min and held at 500 °C for 6 h and quenched into water.

All alloys were immediately aged at 200 °C in an oil bath for various lengths of time after solution treatment and the age hardening response was measured using Vickers hardness measurements (10 kg). Each reported measurement was the average of at least 6 individual measurements. Thin foil specimens for transmission electron microscopy (TEM) were prepared by punching 3 mm diameter discs and electropolishing using a solution containing LiCl, $MgClO_3$ and 2-buytoxy ethanol in methanol at −45 °C, 0.125 A and 100 V. The microstructural examination was conducted on a Philips CM20 TEM operating

Table 1
Alloy compositions studied (at.%)

Base alloy	Zn-modified alloys	Cumulative effect alloy
Mg–1.3 Sn	Mg–1.3 Sn–0.4 Zn, Mg–1.3 Sn–1.2 Zn	Mg–1.3 Sn–1.2 Zn–0.13 Na

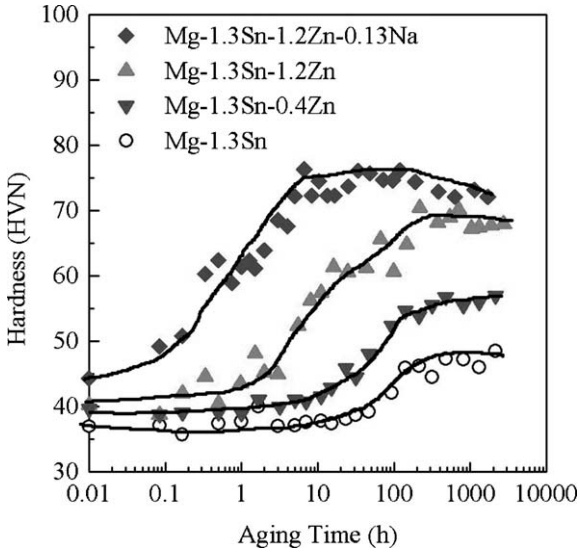

Fig. 2. Isothermal aging curves at 200 °C for the binary Mg–1.3 Sn alloy, the two ternary alloys with additions of 0.4 and 1.2 Zn, and the quaternary alloy with Zn and Na additions.

Table 2
Time to reach maximum hardness, maximum hardness recorded and the increment of hardness due to precipitation hardening

Alloy composition (at.%)	Time to reach peak hardness (h)	Maximum hardness (VHN)	Maximum increment in hardness (VHN)
Mg–1.3 Sn	~1000	47	10
Mg–1.3 Sn–0.4 Zn	300	56.8	16.8
Mg–1.3 Sn–1.2 Zn	211	70.1	30
Mg–1.3 Sn–0.12 Na [5]	58	63.2	26.8
Mg–1.3 Sn–1.2 Zn–0.19 Na	6.7	76.4	31.5

at 200 kV. The thickness of the foils, for the calculation of precipitate number density, was determined using CBED analysis [28].

3. Results

3.1. Base alloy: Mg–1.3 Sn (at.%)

The age hardening response of the binary alloy at 200 °C is shown in Fig. 2, and the important features of the response are presented in Table 2. It is clear that the aging kinetics at this temperature are sluggish (requiring in excess of 200 h to reach peak hardness) and that the hardening increment is poor, being only of the order of 10 VHN.

The peak-aged microstructure is shown in Fig. 3. The equilibrium Mg_2Sn phase is the only precipitating phase, existing as lath-like particles on the basal plane, elongated in the $\langle 1\,1\,\bar{2}\,0\rangle_{Mg}$ directions. The mean dimensions and aspect ratios are given in Table 3, together with an estimated precipitate number density of $0.6 \times 10^{18}\ m^{-3}$. A detailed description of the microstructure

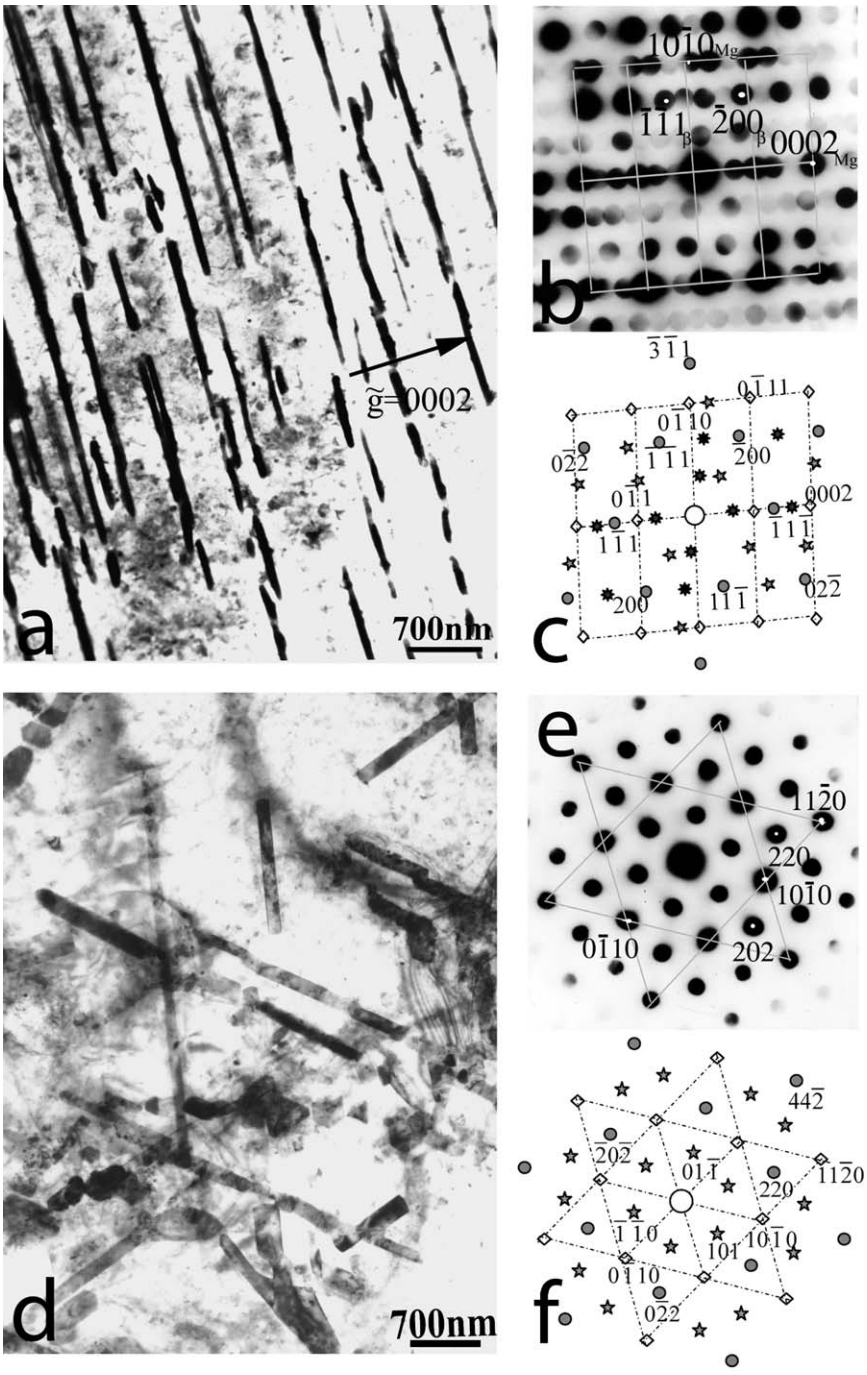

Fig. 3. TEM micrographs of the peak aged microstructure of the Mg–1.3 Sn alloy in the (a) $\langle 1\,1\,\bar{2}\,0\rangle_{Mg}$ and (d) $[0\,0\,0\,1]_{Mg}$ beam directions. The respective microbeam diffraction patterns from the precipitates are shown in (b) and (d), together with an interpretation of the patterns in (c) and (f), from which the precipitates are identified as Mg_2Sn.

Table 3
Quantitative microstructural measurements of the alloys investigated by TEM at maximum hardness at 200 °C

Alloy composition (at.%)	N_v ($\times 10^{18}$ m^{-3})	$\bar{l}$ (nm)	$\bar{w}$ (nm)	$\bar{t}$ (nm)	$\bar{l}/\bar{w}$	$\bar{l}/\bar{t}$
Mg–1.3 Sn	0.60	1500 ± 400	500 ± 80	54 ± 11	3	28
Mg–1.3 Sn–1.2 Zn						
Basal laths	1.35	650 ± 55	320 ± 45	60 ± 25	2	11
$[0\,0\,0\,1]_{Mg}$ laths	1.05	1105 ± 324	–	180 ± 55		6
Mg–1.3 Sn–0.15 Na [5]	56.4	230 ± 50	90 ± 22	25 ± 8.5	2.55	9.2
Mg–1.3 Sn-1.2 Zn–0.19 Na	81.5	70 ± 25	63 ± 15	25 ± 6.8	1.1	2.8

is given elsewhere [5], with the OR obtained by Derge et al. [4] being confirmed.

3.2. Zn-modified alloys: Mg–1.3 Sn–0.4 Zn and Mg–1.3 Sn–1.2 Zn (at.%)

The hardening response of the Mg–1.3 Sn–0.4 Zn and Mg–1.3 Sn–1.2 Zn alloys as a function of aging time at 200 °C is shown in Fig. 2, and the salient features reported in Table 2. The as-quenched hardnesses of the ternary alloys are very similar to those of the binary alloy, and the time to reach peak hardness is relatively unaffected by the Zn additions. However, the hardening increment is greatly improved, with the addition of 1.2 at.% Zn leading to a three-fold increase over that observed in the binary alloy, and the incubation period before the hardness begins to increase is reduced from ∼10 h in the binary and low Zn alloys to ∼0.2 h in the alloy containing 1.2 at.% Zn.

The microstructure in the Mg–1.3 Sn–1.2 Zn alloy has been examined using TEM (Figs. 4 and 5) and the structure corresponding to the peak aged state shows significant changes in particle morphology and habit from those in the binary alloy. At least three families of particles are observed: lath-like precipitates formed on the basal planes of the matrix (Type 1), similar in shape and form to those observed in the binary alloy, lath-like precipitates on prismatic planes (Type 2) elongated in $[0\,0\,0\,1]_{Mg}$ directions with an $\bar{l}/\bar{t}$ ratio approximately half that of Type 1 precipitates, and laths forming on pyramidal

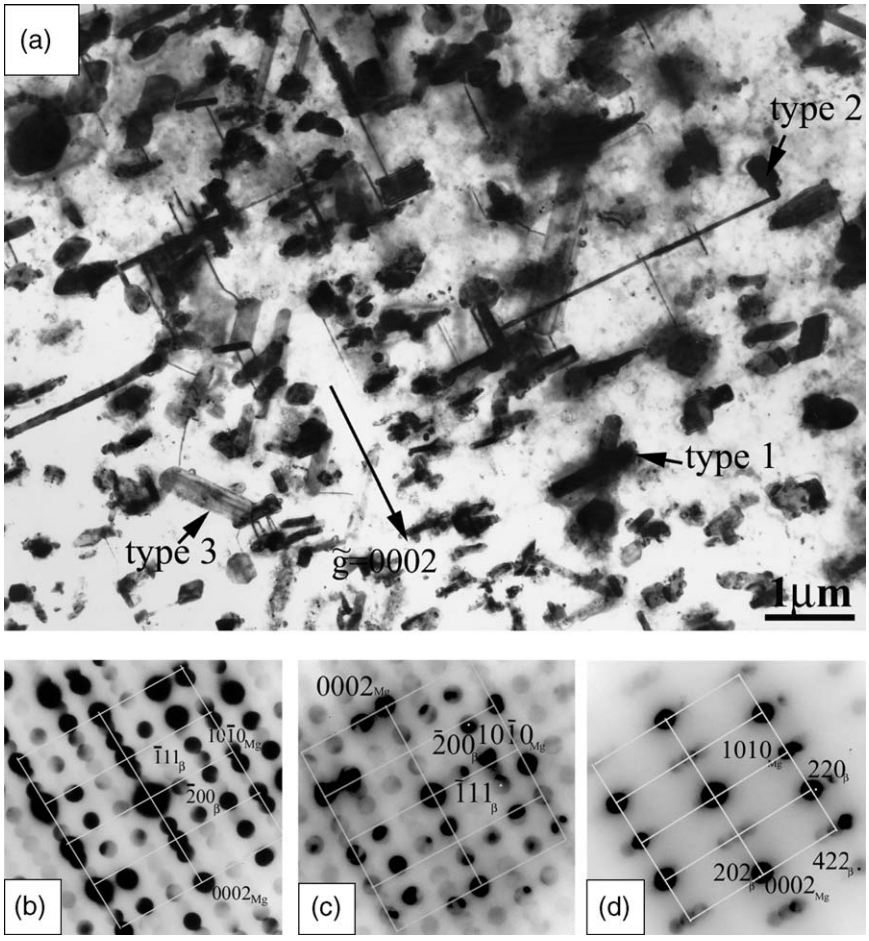

Fig. 4. TEM micrograph of the peak aged microstructure of the Mg–1.3 Sn–1.2 Zn alloy in the (a) $\langle 1\,1\,\bar{2}\,0\rangle_{Mg}$ beam direction, identifying three main precipitate types. The respective microbeam diffraction patterns from the three precipitate variants are shown, with interpretation, in (b), (c) and (d).

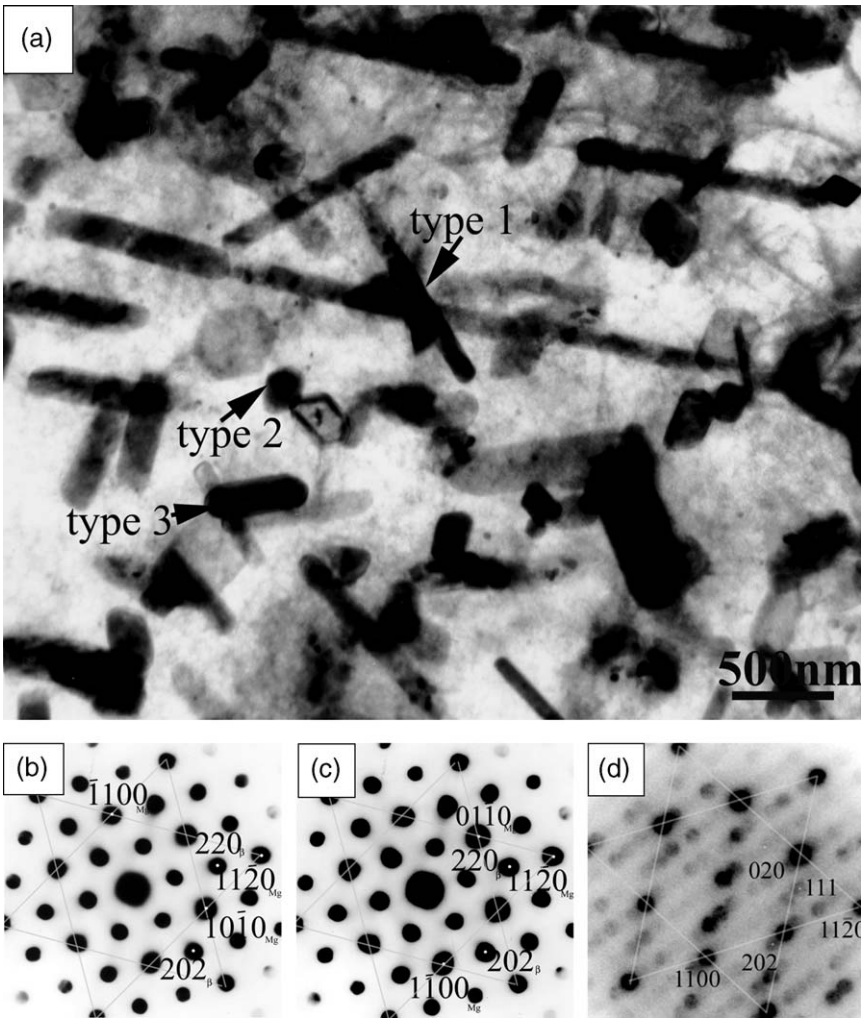

Fig. 5. TEM micrograph of the peak aged microstructure of the Mg–1.3 Sn–1.2 Zn alloy in the (a) $[0\,0\,0\,1]_{Mg}$ beam direction, identifying the three main precipitate types. The respective microbeam diffraction patterns from the three precipitate variants are shown, with interpretation, in (b), (c) and (d).

planes (Type 3). Figs. 4 and 5 are TEM micrographs taken from $\langle 1\,1\,\bar{2}\,0\rangle_{Mg}$ and $[0\,0\,0\,1]_{Mg}$ beam directions, respectively, and microdiffraction patterns taken from the three precipitate families. All three precipitate types have been identified as Mg_2Sn. Types 1 and 2 have the same orientation relationship as described for the binary alloy (Eq. (1)). However, their growth directions are completely different. Type 1 precipitates are elongated in $\langle 1\,1\,\bar{2}\,0\rangle_{Mg}$ directions within in the basal plane (as in the binary alloy; Fig. 3) whereas Type 2 precipitates are elongated in $[0\,0\,0\,1]_{Mg}$ directions. The less prevalent Type 3 precipitates have a $\{1\,0\,1\}_{Mg_2Sn}//(0\,0\,0\,1)_{Mg}$ and $\langle 1\,1\,1\rangle_{Mg_2Sn}//\langle 1\,1\,\bar{2}\,0\rangle_{Mg}$ type relationship.

Types 1 and 2 precipitates dominate the microstructure. The size and distribution of these two families have been measured, and are summarized in Table 3. There is a modest increase in the number of precipitates on the basal planes (approximate doubling of the number density over that observed in the binary alloy) and a refinement in the precipitate length and width, but no significant change in the thickness. From a hardening point of view, the more significant modification is the appearance of the second family of Mg_2Sn laths (Type 2) in almost equal numbers elongated in $[0\,0\,0\,1]_{Mg}$ directions. These laths are longer and thicker than those on the basal plane.

It should be noted that the microstructure in this alloy is complex and at this stage only the dominant features have been discussed. The precipitates on the pyramidal planes (Type 3) have been identified but not fully characterised, and a very small number of MgZn precipitates have also been observed.

3.3. Cumulative effect alloy: Mg–1.3 Sn–1.2 Zn–0.13 Na (at.%)

The age hardening response of this alloy is also shown in Fig. 2, and the relevant features are recorded in Table 2. The as-quenched hardness of the alloy is ∼10% higher than that observed in the non-Na containing alloys, and the response to aging is both enhanced and accelerated compared with the Mg–1.3 Sn–1.2 Zn alloy. The hardening increment is 3.2 times that of the binary Mg–Sn alloy, although only 1.05 times that of the comparable Mg–Sn–Zn ternary alloy. The time to reach peak hardness has, however, been reduced by a factor of 30 (to a much more commercially attractive 7 h) compared with the

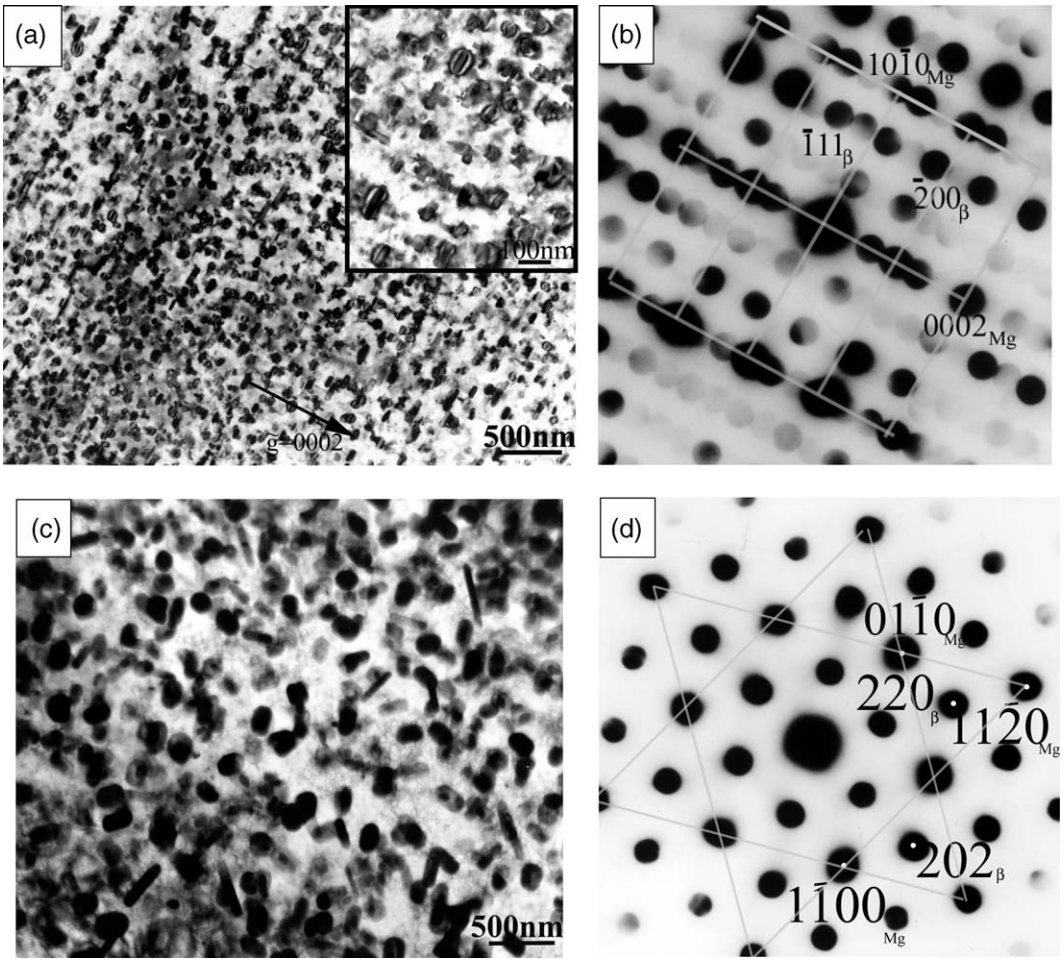

Fig. 6. TEM micrographs of the peak aged microstructure of the quaternary Mg–1.3 Sn–1.2 Zn–0.12 Na alloy in the (a) $\langle 1\,1\,\bar{2}\,0\rangle_{Mg}$ and (c) $[0\,0\,0\,1]_{Mg}$ beam directions. The inset in (a) highlights the refinement in scale and the strain associated with the precipitates. The respective microbeam diffraction patterns from the precipitates are shown, with interpretation, in (b) and (d).

ternary Mg–1.3 Sn–1.2 Zn alloy and the incubation period for the beginning of the rise in hardness has been further reduced to a matter of a few minutes.

Examination of the microstructure using TEM (Fig. 6) shows both a significant refinement in particle distribution and a change in particle morphology (Table 3). There was only one family of precipitates, which was identified as the equilibrium Mg_2Sn phase with the $\{1\,1\,1\}_{Mg_2Sn}//(0\,0\,0\,1)_{Mg}$ and $\langle 1\,1\,0\rangle_{Mg_2Sn}//\langle 1\,1\,\bar{2}\,0\rangle_{Mg}$ OR found in the binary alloy (Eq. (1)). The particles are, however, much more equiaxed, with an $\bar{l}/\bar{w}$ of 1.1 and an $\bar{l}/\bar{t}$ of 2.8. The enlarged inset within Fig. 6(a) attempts to illustrate the refinement of scale and the level of strain contrast around the individual particles. The number density was measured as 8×10^{19} m^{-3}, which is an increase of two orders of magnitude over the binary alloy (Table 3).

4. Discussion

This work was intended to determine if it was possible to use alloying additions specifically to modify precipitate morphology and to check if such an approach could be used in conjunction with recently developed approaches to increasing strength through particle refinement using microalloying additions [5]. The Mg–Sn system is an ideal candidate for such manipulations: the solid solubility declines rapidly as the temperature is reduced and the single equilibrium phase reportedly can have different orientation relationships with the matrix depending on aging temperature. However, the age hardening response of the binary alloy is poor.

Additions of Zn to the binary Mg–Sn alloy led, in total, to a four-fold increase in the number of precipitates (a modest effect compared with Na additions) but provided opportunities for multiple orientation relationships and preferred growth directions. Growth along the $\langle 1\,1\,\bar{2}\,0\rangle_{Mg}$ directions was apparently restricted in the basal precipitates, and growth along $[0\,0\,0\,1]_{Mg}$ was promoted in the prismatic precipitates. Derge et al. [4] have reported the existence of several orientation relationships, depending on the aging temperature. Variations of the lattice correspondence across the precipitate/matrix interface (and therefore the lattice parameter ratios) will affect the relative mobility of the interphase interfaces of the precipitate but the diffusional processes accompanying interface migration should also be considered and much more work is required to understand the observed changes in particle morphology and orientation. Additions of Zn will certainly alter the lattice parameters and

may alter the character of the material in the immediate vicinity of the precipitate/matrix interfaces—there are no reported observations of Zn atom substitution in the Mg_2Sn lattice and as precipitation occurs Zn may be rejected from the growing precipitate. The net effect observed experimentally appears to be that growth in directions both parallel and perpendicular to the basal plane is equally favoured.

It has previously been shown [5] that trace additions of Na to a Mg–1.3 Sn binary alloy refine the precipitate distribution by 2 orders of magnitude and increase the hardening increment by a factor of 2.7. The kinetics of the aging response was improved (time to peak hardness was reduced from >200 h in the binary alloy to 58 h) and the incubation period was extremely short but the peak-aged microstructure was not stable and overaging was relatively rapid [5].

In looking at the hardening increments possible through either Na [5] or Zn additions, it may be said that the addition of 0.12 at.% Na has approximately the same hardening effect as an addition of 1.2 at.% Zn (Table 2), but the mechanisms through which these are achieved are very different. The Na additions have a pronounced effect on the number density of precipitates and this is the principle mechanism for increasing the hardness [5]. Zn additions had only a small effect on the number density of precipitates but had a large effect on the shape of the particles with respect to the basal plane. The primary origin of the hardening observed with Zn additions is thought to lie in the modifications to particle morphology with respect to basal slip and the resulting variations in the probability of dislocations interacting with these precipitates.

The quaternary alloy contained both Na and Zn additions, and the cumulative effect is especially interesting. The refining effect of the Na has been retained (Fig. 6), and the precipitates maintain the dominant OR (Eq. (1)). Growth of the precipitates has been restricted to an even greater extent than in the binary alloy with Zn, such that the length and width dimensions are essentially equal and there is no obvious preferred growth direction. The most interesting effects of the combined additions are in the kinetics of aging and the stability of the precipitating Mg_2Sn phase. Additions of Zn to the binary Mg–Sn alloy resulted in an enhanced hardening without significant effects on the time to peak hardness. Additions of Na result in significant reductions in the time to peak hardness and an enhanced response [5]. Cumulative additions resulted in a further enhancement in hardness and a further significant *reduction* in the time to peak hardness. A synergistic effect of Na and Zn on the time to peak hardness is observed (Table 2). The mechanism underlying this effect is not clear at this stage. In addition, the peak hardness in the alloy containing both Na and Zn additions alloy is very stable, being maintained to beyond 3000 h, and the rapid overaging observed in the binary alloy with Na [5] has been suppressed. This is even though the number density of particles in the quaternary Mg–Sn–Zn–Na alloy is *greater* (and therefore on average the particles are smaller) than that formed in the ternary Mg–Sn–Na alloy. More work is required to identify the physical origin of this enhanced stability, but it is likely that the interfacial energy is significantly reduced, probably through interfacial segregation, resulting in a reduced driving force for coarsening processes. Further work is required to fully characterise the interfaces and the mechanisms leading to the enhanced stability.

5. Conclusions

Additions of Zn to a Mg–1.3 Sn (at.%) alloy are shown to have a significant effect on the age hardening behavior at 200 °C. The times to peak hardness are relative unaffected but the increment in hardening from precipitates is increased threefold. Transmission electron microscopy observations reveal only modest increases in the number density of particles but significant changes in particle morphology are observed. The enhanced hardening response is attributed to the change in particle morphology and the increased probability of these precipitates interacting with dislocation gliding on basal planes.

Combined additions of Na (an element previously shown to be an effective microalloying element for the Mg–Sn system) and Zn result in further enhancements in the age hardening response and substantial accelerations in the time to peak hardness at 200 °C. Microstructural examination reveals a large increase in the number density of particles (an effect characteristic of Na additions) and a change in the particle morphology (an effect characteristic of Zn additions). However, synergistic effects are also observed. The thermal stability of the resulting particle distribution is greatly enhanced compared with the distribution usually observed in Mg–Sn–(Na) alloys even though the number density of particles is greater than what is typically observed in the ternary Na containing alloys. The time to peak hardness in the quaternary alloys is also much shorter than observed in the ternary Na containing alloys (7 h compared with 58 h). The physical origins underlying these synergistic effects are not clear at this stage.

Acknowledgements

This work is supported by the CAST CRC. CAST CRC was established under and is supported by the Australian Government's Cooperative Research Centres Scheme. CRH and CLM acknowledge support from the Australian Research Council (ARC) under the Discovery Projects scheme (CRH; Project ID: DP0557517) and as part of the ARC Centre of Excellence for Design in Light Metals. CRH also gratefully acknowledges the support of Monash University in the form of a University Fellowship.

References

[1] P. Villars, L.D. Calvert, Pearson's Handbook of Crystallographic Data for Intermetallic Phases, ASM International, Materials Park, 1991.
[2] A.L. Bowles, H. Dieringa, C. Blawert, N. Hort, K.U. Kainer, Mater. Sci. Forum 488/489 (2005) 135.
[3] J. van der Planken, J. Mater. Sci. Lett. 4 (1969) 927.
[4] G. Derge, A.R. Kommell, R.F. Mehl, Trans. AIME 124 (1937) 367.
[5] C.L. Mendis, C.J. Bettles, M.A. Gibson, S. Gorsse, C.R. Hutchinson, Philos. Mag. Lett., in press.
[6] A.J. Ardell, Metall. Trans. A 16 (1985) 2131.
[7] L.M. Brown, R.K. Ham, Strengthening Methods in Crystals, Applied Science Publishers, London, 1971.

[8] B. Reppich, in: R.W. Cahn, P. Haasen, E.J. Kramer (Eds.), Mater. Sci. Tech., VCH Verlagsgesellschaft mbH, Weinheim, 1993, p. 311.
[9] B.C. Muddle, S.P. Ringer, I.J. Polmear, Trans. Mater. Res. Soc. Jpn. 19B (1994) 999.
[10] I.J. Polmear, Mater. Forum 23 (1999) 117.
[11] H.K. Hardy, J. Inst. Met. 80 (1952) 483.
[12] J.M. Silcock, T.J. Heal, H.K. Hardy, J. Inst. Met. 84 (1955) 23.
[13] S.P. Ringer, K. Hono, T. Sakurai, Metall. Mater. Trans. A 26 (1995) 2207.
[14] L. Bourgeois, J.F. Nie, B.C. Muddle, Philos. Mag. 85 (2005) 3487.
[15] I.J. Polmear, Trans. AIME 230 (1964) 1331.
[16] L. Reich, M. Murayama, K. Hono, Acta Mater. 46 (1998) 6053.
[17] J.W. Martin, R.D. Doherty, B. Cantor, Stability of Microstructure in Metallic Systems, Cambridge University Press, Cambridge, 1997.
[18] I.M. Lifshitz, V.V. Slyozov, J. Phys. Chem. Solids 19 (1961) 35.
[19] C. Wagner, Z. Elektrochem. 65 (1961) 581.
[20] C.R. Hutchinson, J.F. Nie, S. Gorsse, Metall. Mater. Trans. A 36A (2005) 2093.
[21] P.G. Partridge, Metall. Rev. 12 (1967) 169.
[22] J.F. Nie, Scripta Mater. 48 (2003) 1009.
[23] M.X. Zhang, P.M. Kelly, Acta Mater. 53 (2005) 1073.
[24] M.X. Zhang, P.M. Kelly, Acta Mater. 53 (2005) 1085.
[25] W.Z. Zhang, G.C. Weatherly, Prog. Mater. Sci. 50 (2005) 181.
[26] J.F. Nie, Acta Mater. 52 (2004) 795.
[27] A.A. Nayeb-Hashemi, J.B. Clark, Phase Diagrams of Binary Magnesium Alloys, ASM International, Metals Park, 1988.
[28] D.B. Williams, C.B. Carter, Transmission Electron Microscopy: A Textbook for Materials Science, Plenum Press, New York, 1996, p. 321.